COMMUNICATIONS CHEMISTRY

ARTICLE

DOI: 10.1038/s42004-018-0044-9 OPEN

Trace mono-atomically dispersed rhodium on zeolite-supported cobalt catalyst for the efficient methane oxidation

Yuhui Hou [1], Shinichi Nagamatsu[1], Kiyotaka Asakura [1], Atsushi Fukuoka [1] & Hirokazu Kobayashi [1]

The partial oxidation of methane is a promising method for the efficient production of syngas. To implement this process using common stainless steel reactors, an inexpensive catalyst that functions at 650 °C or below is necessary. However, base metal catalysts typically require much higher temperatures, and they are deactivated by re-oxidation and coke formation. Here we report that modification of a zeolite-supported 3 wt% cobalt catalyst with a trace amount of mono-atomically dispersed rhodium (0.005 wt%) dramatically improves catalytic performance and durability. Cobalt/mordenite is nearly inactive due to the oxidation of cobalt, but the catalyst modified with rhodium continuously gives 85–86% methane conversion and 90–91% CO selectivity with an H_2/CO ratio of 2.0 without serious coking at 650 °C. During the reaction, mono-atomically dispersed rhodium converts cobalt oxide to Co^0 active species via hydrogen spillover. Use of the zeolite support is key to the high catalytic performance.

[1] Institute for Catalysis, Hokkaido University, Kita 21 Nishi 10, Kita-ku, Sapporo, Hokkaido 001-0021, Japan. Correspondence and requests for materials should be addressed to H.K. (email: kobayashi.hi@cat.hokudai.ac.jp)

The conversion of methane to liquid fuels and chemicals by heterogeneous catalysis has attracted increased interest since the shale gas revolution, due to the enhanced availability of methane and increasing global demands of power sources[1–4]. Methane-derived chemicals such as hydrocarbons and methanol are manufactured via syngas, a mixture of CO and H_2. The economical synthesis of higher alcohols from syngas to produce polymers, pharmaceuticals, and energy carriers is also a hot topic[5]. Accordingly, the efficiency of syngas production is a critical factor to determine the economics of methane utilisation. Syngas is produced by the catalytic conversion of methane with H_2O, CO_2, or O_2, where the reaction becomes exothermic only when O_2 is involved[6]. The partial oxidation of methane (POM) with O_2 to syngas allows the use of compact facilities in industry due to the favourable thermodynamic properties and because a water vapour supply is unnecessary. This is in contrast to the steam-reforming of methane that requires a very large-scale process to be economical[7].

Catalysts for POM to syngas can be classified into two types: noble metals and base metals. Noble metal catalysts such as Rh and Pt show higher catalytic activities and work at lower temperatures, compared to base metal catalysts[8–12], but noble metals are more costly. On the other hand, while base metals are inexpensive, they require pre-reduction, and high reaction temperatures above 800 °C (for the actual temperature of the catalyst bed) to achieve high selectivity. This high temperature exceeds the range in which common industrial stainless steel reactors can be used, specifically 650 °C or lower. Moreover, base metal catalysts are often deactivated by severe coking and re-oxidation during the reaction[13–15]. Thus, these issues with base metals often result in a high long-term cost.

A combination of base metals and noble metals is one solution to overcome these obstacles. The addition of noble metals facilitates the reduction of base metals and inhibits their re-oxidation. Rh is particularly effective for this purpose[16–18]. The amount of Rh on catalysts reported so far is typically more than 0.3 wt%. Although a catalyst of 0.005 wt% Rh–3.0 wt% NiO_x/Al_2O_3 showed higher activity and selectivity than monometallic Rh or Ni catalysts, it still required a temperature of 800 °C to maintain its activity[19]. The catalyst was deactivated at lower temperatures, perhaps by re-oxidation due to the stabilisation of the oxide phase as $NiAl_2O_4$[20]. Accordingly, it is a challenge to develop a base metal catalyst containing only a trace amount of noble metals for low-temperature POM.

In this work, we prepare highly dispersed Co particles (1.5 nm) modified with 0.005 wt% Rh on a mordenite (MOR) zeolite. The catalyst converts methane to syngas with up to 91% selectivity and 86% conversion at 650 °C with good durability. Mechanistically, mono-atomically dispersed Rh on Co particles maintains the Co^0 state via hydrogen spillover during POM. The small Co^0 particles (1.5 nm) not only provide high activity but also inhibit the formation of coke. The use of zeolite as a support is the key for good reducibility and high dispersion of Co. Other supports tested cannot achieve these features.

Results

Characterisation of catalysts. We prepared 3 wt% Co/MOR, 0.005 wt% Rh/MOR, and 0.005 wt% Rh–3 wt% Co/MOR, denoted Rh–Co/MOR, by simple impregnation methods. The loading amount of Rh was optimised as 0.005 wt% (Supplementary Fig. 1). MOR was chosen as a typical zeolite in this study since MOR, beta, and ZSM-5 zeolites showed similar catalytic activities in a screening test (Supplementary Fig. 2). The zeolite framework structures were confirmed by physicochemical techniques. In the X-ray diffraction (XRD) analysis, all the samples exhibited only characteristic diffraction lines of MOR (Supplementary Fig. 3). The intensity and width of the peaks were similar before and after the impregnation of metal species. Diffraction peaks for Rh or Co species were not detected due to the low content of Rh (0.005 wt%), high dispersion, or amorphous nature. N_2 adsorption/desorption isotherms of pristine MOR and the catalysts (Supplementary Fig. 4) were all of the type I form, characteristic of microporous materials. The Brunauer–Emmet–Teller (BET)-specific surface area of original MOR was 520 $m^2\,g^{-1}$, and the value decreased slightly after loading of Rh and Co (490–500 $m^2\,g^{-1}$; Supplementary Table 1). MOR and the prepared catalysts had similar micropore volumes (0.18–0.19 $cm^3\,g^{-1}$). These results indicate no collapse or blockage of the MOR micropores.

High-angle annular dark-field scanning transmission electron microscopy (HAADF-STEM) was employed to determine the particle size of the Co and Rh species. Bright dots were observed for Rh–Co/MOR (Fig. 1a) with a mean particle diameter of 1.5 nm (Fig. 1d). Energy dispersive X-ray (EDX) analysis at the bright dots showed strong signals of Co Kα (6.92 keV) and Lα (0.776 keV), but no signal of Rh (Supplementary Fig. 5), indicating that the particles predominantly consisted of Co. Furthermore, the dark spots gave only O, Al, and Si peaks ascribed to the MOR support (Supplementary Fig. 6). Rh species could not be detected due to their low concentration (0.005 wt%). Co/MOR had particles of Co species with an average diameter of 1.5 nm (Fig. 1b, e; EDX Supplementary Fig. 7), which was similar to that of Rh–Co/MOR. Thus, the co-impregnation of 0.005 wt% Rh did not change the dispersion of Co.

The oxidation state of the Co species on Rh–Co/MOR and Co/MOR was determined by Co 2p X-ray photoelectron spectroscopy (XPS; Fig. 2). Both samples exhibited four peaks assigned to Co $2p_{3/2}$, $2p_{1/2}$, and their satellite peaks. The presence of strong satellite peaks is evidence for high-spin Co^{2+} species. The position of Co $2p_{3/2}$ (782 eV) and ΔE to its satellite peak (5.3 eV) are similar to those of $Co(OH)_2$ or CoO supported on oxides[21–23]. Further analysis by Co K-edge X-ray absorption fine structure (XAFS) confirmed the presence of Co^{2+} and the coordination of O to Co (Supplementary Fig. 8 and Supplementary Table 2). The particles containing the Co^{2+} species are hereafter referred to as Co oxide particles. Comparing the XPS spectra for Co/MOR and Rh–Co/MOR, we found no influence of Rh on the peak positions due to the low loading of Rh (0.005 wt %). Note that Rh is undetectable by XPS for the same reason.

We studied the effect of the trace amount of Rh on the reduction of Co oxide by temperature-programmed desorption (TPR; Fig. 3). Original MOR and Rh/MOR exhibited no H_2 consumption peaks over the temperature range of 100–870 °C. The lack of a visible reduction peak for Rh/MOR was due to the low loading of Rh (0.005 wt%). Co/MOR showed two main peaks at around 320 and 780 °C. The former peak is assigned to the reduction of typical Co oxide[24,25]. The latter peak is attributed to Co oxide species directly interacting with MOR, such as Co atoms at the boundary with the support in Co oxide particles[24]. The temperature of the two peaks decreased by 50–100 °C by adding Rh. Hence, Rh assists in the reduction of Co oxide, which implies that Rh interacts with Co.

The TPR study motivated us to investigate whether Rh and Co species were present in close proximity or in isolation. Because of the very low concentration of Rh (0.005 wt%) and large excess of Co (3.0 wt%), fluorescence XAFS of Rh is the most promising source to obtain such information. Thus, we analysed Rh K-edge X-ray absorption near-edge structure spectra of two samples, pristine Rh–Co/MOR and Rh–Co/MOR reduced by H_2 without exposure to air, to reproduce the chemical state of the catalyst under POM (see below). The pristine Rh–Co/MOR gave an edge energy of 23,224 eV, similar to that of Rh_2O_3 (Fig. 4). The edge

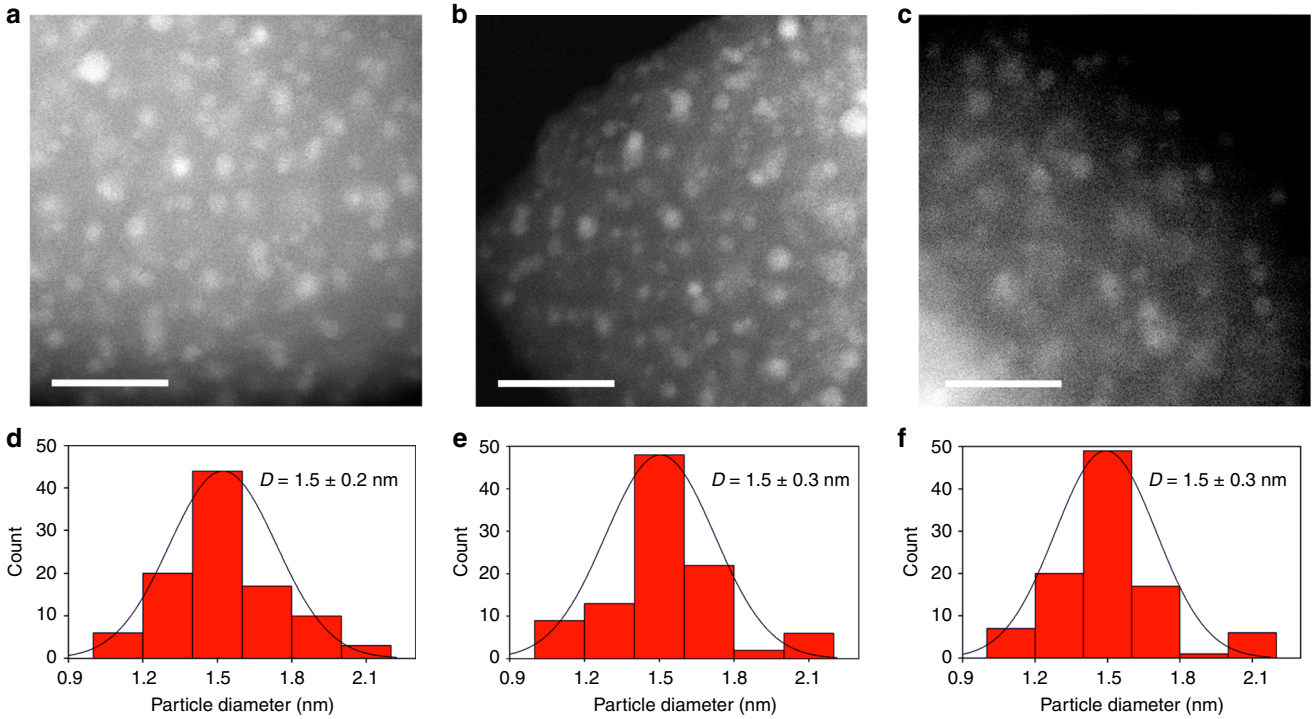

Fig. 1 High-angle annular dark-field scanning transmission electron microscopy images of catalysts and particle size distributions. Rh–Co/MOR (**a**, **d**), Co/MOR (**b**, **e**), and spent Rh–Co/MOR after the partial oxidation of methane at 650 °C for 50 h (**c**, **f**). Scale bars in **a**–**c**: 10 nm

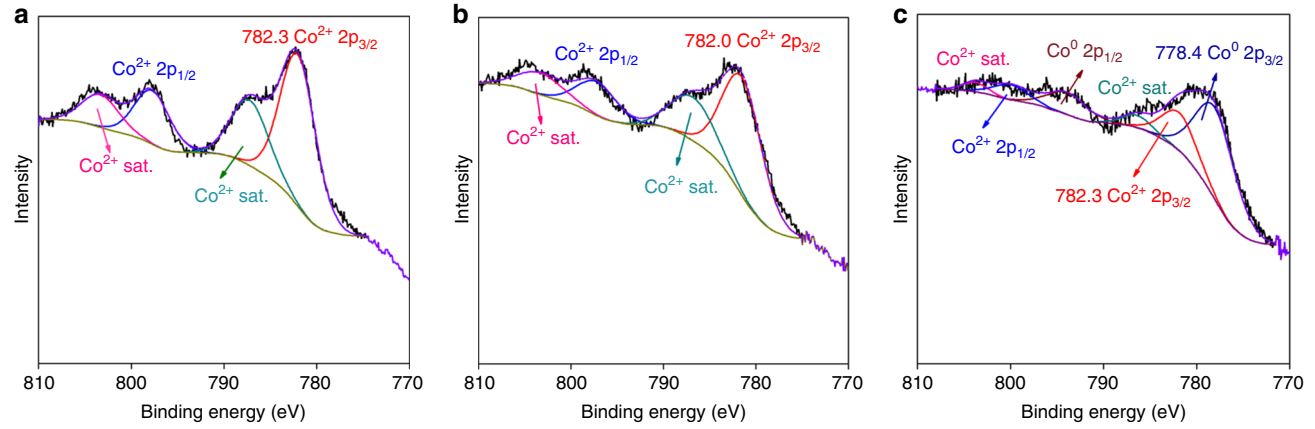

Fig. 2 Co 2p X-ray photoelectron spectra of catalysts. Rh–Co/MOR (**a**), Co/MOR (**b**), and spent Rh–Co/MOR after the partial oxidation of methane at 600 °C for 18 h (**c**). Black line: raw experimental data, coloured lines: curve-fitting data. sat. satellite peak

was shifted to 23,219 eV after the reduction, which was similar or slightly lower than that of Rh foil and reduced Rh/MOR (23,220 eV) (enlarged image: Supplementary Fig. 9). The negative shift is attributed to charge transfer from Co to Rh, as Rh has a higher electronegativity ($\chi_P^{Rh} = 2.28$) than Co ($\chi_P^{Co} = 1.88$).

To clarify the coordination condition of the Rh atoms, we analysed extended X-ray absorption fine structure (EXAFS) spectra of pristine and reduced Rh–Co/MOR. After Fourier transformation of the EXAFS oscillations (Supplementary Fig. 10), pristine Rh–Co/MOR gave two peaks at 1.6 and 2.4 Å as non-corrected distances (Fig. 5). The former peak is assigned to the Rh–O shell, but the latter is different from the Rh–Rh shell for Rh_2O_3. The curve-fitting analysis was successful when a Rh–Co shell was hypothesised for the latter peak, which indicated the presence of 6.4 O atoms at 2.03 Å and 3.4 Co atoms at 2.87 Å (Table 1). Rh–Rh and Rh–Co shells could be distinguished by the clear difference in backscattering amplitude and phase shift. Accordingly, trivalent Rh atoms are located on/in cobalt oxide particles. After the reduction, Rh–Co/MOR exhibited a peak at 2.2 Å as a non-corrected distance in the Fourier transform (Fig. 5), which was also different from that of Rh foil (2.5 Å). This is not due to the presence of the MOR support because reduced Rh/MOR had a peak at 2.5 Å. Assuming a Rh–Co shell, curve-fitting analysis of the EXAFS oscillation for Rh–Co/MOR gave a coordination number of 5.6 and an interatomic distance of 2.52 Å with high consistency (R factor = 0.8%). The low coordination number of Co and absence of a Rh–Rh shell indicate that Rh atoms are mono-atomically dispersed on the surface of Co metal nanoparticles (Supplementary Fig. 11). If Rh atoms were present in the bulk phase of Co metal particles, the coordination number would theoretically be 12, which is not the case.

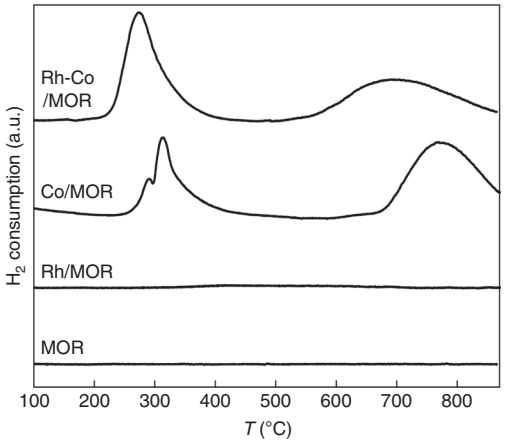

Fig. 3 Temperature-programmed reduction profiles of different samples. Positive peaks indicate the consumption of H_2

POM reaction. The effect of co-impregnation of Rh and Co was evaluated in POM at 600 °C, space velocity (SV) of 60,000 mL h^{-1} g^{-1}, and CH_4/O_2 ratio of 12.5 (Table 2). Definition of conversion, yield, and selectivity is available in Supplementary Note 1. Original MOR gave only 0.6% conversion of methane and 0.01% yield of CO (entry 1), showing no contamination of active species. Rh–Co/MOR gave the highest conversion of methane (15%) among the catalysts tested (entry 2). The reaction produced CO in 14% yield with 90% selectivity and CO_2 in 1.5% yield. Coke formation on the catalyst was 0.1 wt% after 18 h (Supplementary Table 3), corresponding to 0.0004% yield. Single component catalysts, Rh/MOR and Co/MOR, were significantly less active than Rh–Co/MOR under the same reaction conditions (entries 3 and 4). A physical mixture of Rh/MOR and Co/MOR containing the same amounts of Rh and Co as those in Rh–Co/MOR gave 9.7% conversion and 58% selectivity for CO (entry 5), clearly less active and less selective than Rh–Co/MOR. Accordingly, Rh and Co must be present in close proximity for high catalytic performance.

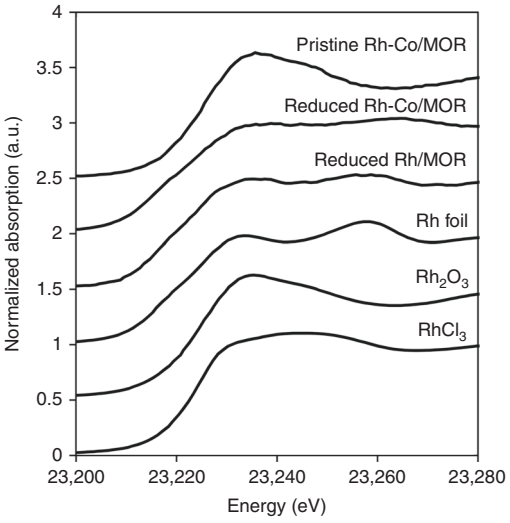

Fig. 4 Rh K-edge X-ray absorption near-edge structure spectra. Edge jumps have been normalized to be 1

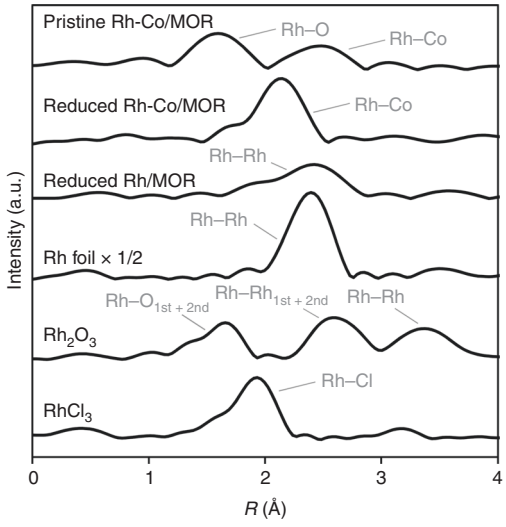

Fig. 5 Fourier transform of Rh K-edge k^3-weighted extended X-ray absorption fine structure spectra. Assignment for shells is shown in gray characters

Table 1 Fitting results of the Rh K-edge EXAFS spectra by FEFF simulations

Sample	Shell	CN[a]	R[b] (Å)	σ^{2c} (Å^2)	R factor (%)
Pristine Rh-Co/MOR	Rh-O	6.4[d]	2.03	0.0012	0.5
	Rh-Co	3.4[d]	2.87	0.0029	
Reduced Rh-Co/MOR	Rh-Co	5.6[e]	2.52	0.0041	0.8
Reduced Rh/MOR	Rh-Rh	4.8[e]	2.66	0.0049	1.1
Rh foil	Rh-Rh	12[e] (12)[f]	2.68 (2.68)[f]	0.0032	1.0
Rh_2O_3	Rh-O_{1st}[g]	3.0[d] (3)[f]	2.03 (2.03)[f]	0.0019	1.2
	Rh-O_{2nd}[g]	3.0[d] (3)[f]	2.07 (2.07)[f]	0.0019	
	Rh-Rh_{1st}[h]	1.0[d] (1)[f]	2.72 (2.72)[f]	0.0018	
	Rh-Rh_{2nd}[h]	3.0[d] (3)[f]	2.99 (2.99)[f]	0.0018	

[a]Coordination number
[b]Interatomic distance
[c]Debye–Waller factor
[d]$S_0^2 = 0.70$, determined by curve-fitting analysis of Rh_2O_3 EXAFS to be consistent with the crystallographic data [e]$S_0^2 = 0.88$, determined by curve-fitting analysis of Rh foil EXAFS to be consistent with the crystallographic data [f]Crystallography
[g]CN, σ^2, and ΔE were fixed to be the same for Rh–O 1st and 2nd shells and the difference in R was fixed at 0.04 Å, based on crystallographic data [h]σ^2 and ΔE were fixed to be the same for Rh–Rh 1st and 2nd shells, CN for Rh–Rh_{2nd} was fixed at three times larger than that for Rh–Rh_{1st}, and the difference in R was fixed at 0.27 Å, based on crystallographic data

Table 2 Catalytic performance of prepared samples in the POM under steady state

Entry	Catalyst	Conv. CH_4 (%)	Yield CO (%)	Yield CO_2 (%)	Sel. CO (%)
1	MOR	0.60	0.01	0.59	2
2	Rh-Co/MOR	15	14	1.5	90
3	Rh/MOR	5.7	2.2	3.4	39
4	Co/MOR	4.6	0.11	4.5	2.5
5	Rh/MOR + Co/MOR[a]	9.7	5.6	4.0	58
6[b]	Rh-Co/SiO_2-Al_2O_3[c]	10	6.3	3.9	62
7[b]	Rh-Co/SiO_2	8.4	5.3	3.1	63
8	Rh-Co/Al_2O_3	8.5	5.0	3.5	59

Reaction conditions: 600 °C, CH_4/O_2/He = 50/4/46, SV = 60,000 mL $h^{-1}g^{-1}$, 0.1 MPa. Loading amounts of Rh 0.005 wt%, Co 3.0 wt%
[a]Physical mixture (1:1). SV = 30,000 mL $h^{-1}g^{-1}$
[b]No steady state due to rapid deactivation by coke formation
[c]Si/Al ratio is the same as that of MOR (45)

The influence of the support was studied by using SiO_2–Al_2O_3, SiO_2, and Al_2O_3. Their characterisation data are shown in Supplementary Figs. 12–17. The three Rh–Co catalysts achieved 8–10% conversion of methane and CO selectivity of ca. 60% (Table 2, entries 6–8), significantly lower than those by Rh–Co/MOR (15% conversion, 90% selectivity, entry 2). SiO_2–Al_2O_3 and SiO_2 produced large particles of Co_3O_4 (12–13 nm), which led to rapid deactivation by serious coking in POM. For example, Rh–Co/SiO_2 produced 2.7 wt% of coke on the catalyst within 2 h. It is known that Co particles of 10–30 nm are active for methane decomposition to C and H_2[26]. Additionally, Co species on Rh–Co/Al_2O_3 were barely reducible (no reduction peak at low temperature in TPR; Supplementary Fig. 17) as reported previously[20,27], thus showing low activity in POM. It is notable that Rh–Co/Al_2O_3 had highly dispersed Co species (TEM; Supplementary Fig. 16) and produced only a small amount of coke (0.12 wt% after 18 h), which is similar to Rh–Co/MOR. Accordingly, metallic Co is active for POM, and high dispersion is crucial to inhibit coke formation.

We carried out the pre-reduction of catalysts with H_2 at 700 °C in order to elucidate the effect of the oxidation state of Co on POM (Fig. 6). Rh–Co/MOR gave almost the same catalytic performance after the pre-treatment. In contrast, the pre-reduction of Co/MOR drastically increased CO selectivity to 91%, although the conversion of methane was only 7.6%, perhaps owing to consumption of some O_2 for the re-oxidation of Co metal. The CO selectivity decreased to 2.5% within 10 min, which was similar to that for the non-reduced catalyst (2.5%). Accordingly, Co^0 is the active species, but it is readily re-oxidised in the absence of Rh under the reaction conditions. Similar deactivation was observed for the physical mixture of Rh/MOR and Co/MOR (Rh/MOR + Co/MOR in Fig. 6). Only Rh–Co/MOR possessed similar activity before and after the reduction. The Co 2p XPS measurement indicated Co^0 as the predominant species for spent Rh–Co/MOR (Fig. 2c), which was in contrast to the spent Co/MOR bearing only Co^{2+} (Supplementary Fig. 18). Hence, Rh–Co/MOR readily produces and preserves metallic Co in the POM reaction.

It is intriguing that Co^0 is formed and preserved in the metallic state by a trace amount of Rh on Rh–Co/MOR in POM. EXAFS and XPS analyses indicate that Rh^{3+} exists within Co oxide particles before the reaction starts. At the beginning of the reaction, zero-valent Rh is produced by the consumption of a stoichiometric amount of methane[12]. The reduced Rh catalyses POM to syngas in small quantities (Table 2, entry 3) and liberates atomic H species either by the dissociation of H_2 formed in POM or from intermediates of POM[28]. The H species can be used for the reduction of Co oxide species. However, most Co oxide particles do not contain any Rh atoms. The average number of Rh

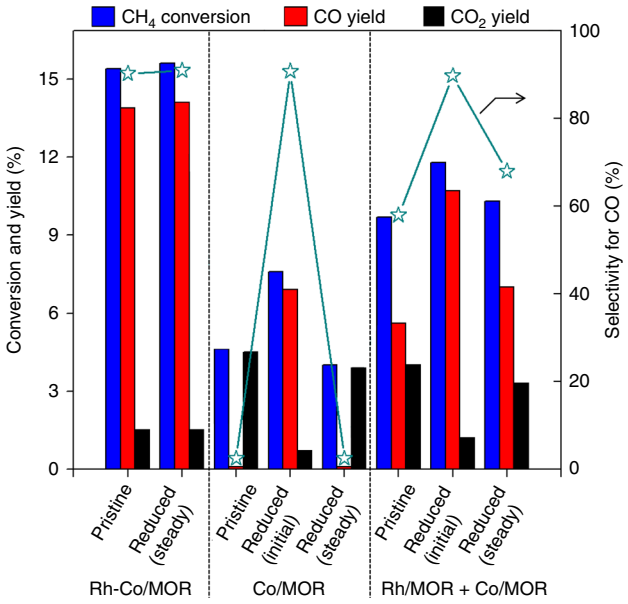

Fig. 6 Effect of reduction of catalysts on the partial oxidation of methane. Conditions: 600 °C, CH_4/O_2/He = 50/4/46, space velocity (SV) = 60,000 mL $h^{-1}g^{-1}$. Reduction was performed under H_2 flow at 700 °C. (initial) indicates the initial activity after reduction; (steady) shows the activity after reaching steady state. Star symbols show the selectivity for CO in the reaction, and lines connecting the symbols guide changes in the selectivity

atoms per Co particle is only 0.11 (Rh:Co atomic ratio = 1:1050, one particle contains ca. 120 Co atoms). To explain this, we propose that atomic H species spill over onto the MOR support and reduce neighbouring Co oxide particles to Co metal (Fig. 7). Choi and co-workers[29,30] demonstrated this hydrogen spillover on an aluminosilicate zeolite, A, in the presence of Pt. The spillover was enhanced by surface Brønsted acid sites, and even a physical mixture of Pt/HA and Al-rich oxide allowed the interparticle hydrogen spillover onto Al-rich oxide to be used for hydrogenation reactions. These results indicate a high mobility of spillover H species on proton-type zeolite. In our case, many Co particles are present within a distance of 2–3 nm to each other on one proton-type MOR particle (Fig. 1a). Thus, it is plausible that the spillover H reduces Co oxide to Co^0 and then maintains its zero-valent state during the reaction. This idea is supported by the TPR experiments that showed a decrease in the reduction temperature of Co when a trace amount of Rh was present (Fig. 3).

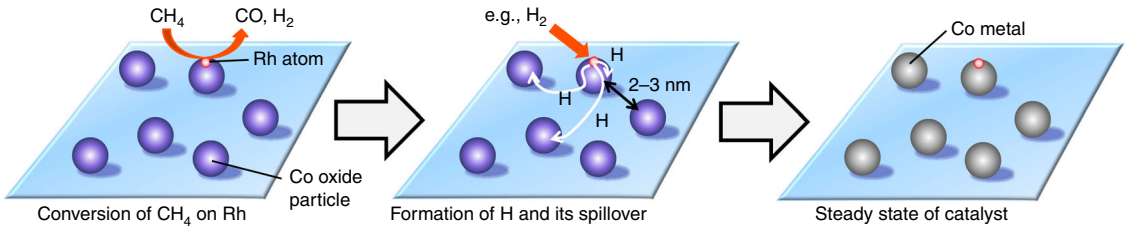

Fig. 7 Conceptual diagram of the proposed reduction of Co oxide by spillover H. Initially, mono-atomically dispersed Rh catalyses the partial oxidation of methane (POM) to syngas in small quantities. Rh liberates atomic H species either by the dissociation of H_2 formed in POM or from intermediates of POM. The H species spill over onto the catalyst support and reduce neighbouring Co oxide particles to Co metal

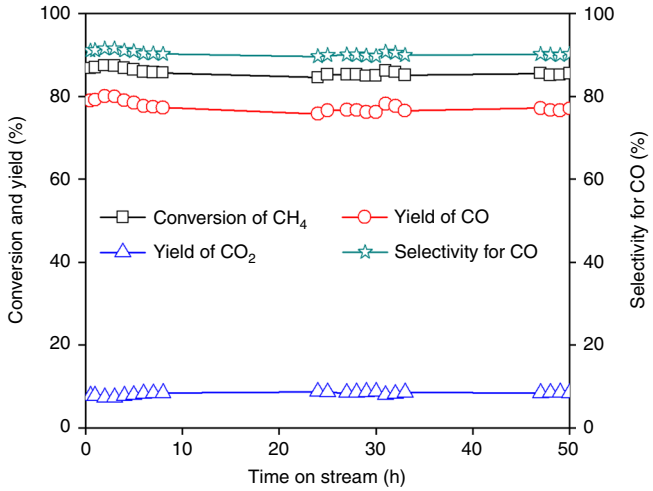

Fig. 8 Durability test of Rh-Co/MOR in the partial oxidation of methane. Conditions: 650 °C, $CH_4/O_2/N_2 = 3.33/1.67/95$, space velocity (SV) = 1,200,000 mL g^{-1} h^{-1}

The long-term stability of catalysts is crucial for the POM reaction. Therefore, a durability test of Rh–Co/MOR was performed at a temperature of 650 °C, CH_4/O_2 ratio of 2, and SV of 1,200,000 mL h^{-1} g^{-1}. The Rh–Co/MOR catalyst steadily provided 85–86% methane conversion and 90–91% CO selectivity over 50 h (Fig. 8). The ratio of H_2/CO was 2.0 in the product, which is the stoichiometric ratio for methanol production and FT synthesis. The produced amount of CO divided by the number of total Co atoms was 120,000 and that of Rh atoms reached 130,000,000, indicating very high productivity. It is noteworthy that neither a structural change of the support nor aggregation of the metal species were observed by XRD (Supplementary Fig. 19) or STEM (Fig. 1c) after the 50 h reaction.

Discussion

The main features of this work are as follows: trace Rh-decorated Co particles with an average diameter of 1.5 nm are formed on MOR zeolite (Rh–Co/MOR) by a simple impregnation method. Rh–Co/MOR is more active, selective, and durable in syngas formation than its monometallic counterparts or their physical mixture. Co oxide on Rh–Co/MOR is spontaneously reduced to form Co^0 active sites in POM, whereas Co/MOR and the physical mixture of Rh/MOR and Co/MOR are not reduced and quickly re-oxidise after H_2 reduction. Controlled experiments and spectroscopic studies suggest that mono-atomically dispersed Rh reduces Co oxide to Co^0 and preserves the zero-valent state in POM via hydrogen spillover for Rh–Co/MOR. Regarding the effect of the catalyst support, Rh–Co bimetallic catalysts using SiO_2–Al_2O_3, SiO_2, and Al_2O_3 as supports have poor durability or lower activity. Large particles of Co (≥10 nm) formed on SiO_2–Al_2O_3 and SiO_2 produce coke, thus showing that the highly dispersed Co species on MOR is essential to inhibit coke formation. Al_2O_3 produces barely reducible cobalt species, giving a lower fraction of Co^0 active species. Thanks to the favourable features of Rh–Co/MOR, the catalyst gives 85–86% methane conversion and 90–91% CO selectivity with an H_2/CO ratio of 2.0 at 650 °C and SV of 1,200,000 mL g^{-1} h^{-1}, and maintains its activity for at least 50 h. The produced amount of CO divided by the number of total Co atoms is 120,000. Consequently, Rh–Co/MOR maintains high activity in POM despite having only a trace amount of Rh. Good reducibility and high dispersion of Co achieved by the MOR support are keys to the high catalytic performance, as other catalyst supports do not provide such attractive features. Zeolites interact with Co species but do not make mixed oxides such as $CoAl_2O_4$, which might result in their favourable features.

Methods

Catalyst preparation. A proton-type MOR with an Si/Al ratio of 45 [JRC-Z-HM90, Catalysis Society of Japan (CSJ)] was used in this study. $Co(NO_3)_2{\cdot}6H_2O$ (0.0764 g, 262 μmol) and 3.88 mM $RhCl_3$ aq. (62.8 μL, 0.24 μmol) were dissolved in 25 mL of water, and then 500 mg of MOR was added into the solution. The mixture was stirred at room temperature for 24 h. A solid material was recovered by evaporation of the mixture at 40 °C under vacuum. The resulting powder was dried at 110 °C overnight and then calcined at 550 °C in air for 6 h to obtain a catalyst labelled as Rh–Co/MOR. The loading amounts of Rh and Co were 0.005 wt% and 3.0 wt%, respectively. The same procedure was adopted for SiO_2–Al_2O_3 (Si/Al = 45), SiO_2 (JRC-SIO-9A, CSJ), and Al_2O_3 (JRC-ALO-8, CSJ) supports.

Catalyst characterisation. XRD patterns were measured by a diffractometer (Ultima IV, Rigaku; Cu Kα 0.154 nm) equipped with a semiconductor array detector (D/teX Ultra 2). BET surface areas of the samples were calculated from N_2 adsorption isotherms at −196 °C recorded on a Belsorp-mini (Microtrac-BEL). Samples were degassed at 200 °C for 3 h under vacuum before measurement. HAADF-STEM images were taken by a JEM-ARM200F (JEOL) equipped with a JED-2300 EDX spectrometer with an acceleration voltage of 200 kV. The Cs-corrector CESCOR (CEOS) was used in the STEM mode. TEM images were obtained by using a JEM-2100F (JEOL) with an acceleration voltage of 200 kV. STEM and TEM samples were prepared by dropping an ethanol suspension of the catalyst on a holey carbon-supported copper grid. STEM and TEM images were displayed using Origin 8 and Paint Shop Pro 4. XPS were acquired on a JPC-9010MC instrument (JEOL) using the Al Kα line. Samples were exposed to air prior to the measurements. TPR was carried out on a Belcat II (Microtrac-BEL) using 5% H_2/Ar mixed gas. Samples for this analysis were treated under He flow at 550 °C for 30 min in advance. Rh K-edge XAFS measurements were carried out in fluorescence mode with a 19-channel Ge solid-state detector at 298 K using synchrotron radiation through an Si (311) double-crystal monochromator at the NW10A beam line on Photon Factory Advanced Ring (PF-AR; ring energy 6.5 GeV, 60 mA) (Proposal Nos. 2016G546 and 2017G624). XAFS spectra were analysed with a REX2000 (Rigaku). EXAFS spectra were extracted with a spline smoothing method. For the curve-fitting analysis, the backscattering amplitude and the phase shift were derived from FEFF 8.40 calculations.

Partial oxidation of methane. The POM was conducted in a quartz fixed-bed flow reactor (inner diameter ø7). The temperature inside the catalyst bed was monitored by a thermocouple (ø0.5). The catalyst was heated to the desired temperature under He flow (9.2 mL min^{-1}). Afterward, the reaction gas mixture (typically, CH_4 10.0 mL min^{-1}, O_2 0.8 mL min^{-1}, He 9.2 mL min^{-1}) was fed into

the reactor. A low concentration of O_2 was used to avoid the formation of hot spots[31], and only a small increase in temperature in the catalyst bed occurred (5–20 °C, depending on reaction conditions). When performing the reaction at a very high SV of 1.2×10^6 mL h^{-1} g^{-1}, the catalyst was diluted twice with MOR (5 mg catalyst, 5 mg MOR) to obtain reliable data. Products were analysed by an on-line gas chromatograph (Shimadzu GC-8A, thermal conductivity detector, Shincarbon ST and molecular sieve 5 A packed columns). The carbon balance calculated from the amounts of methane, CO, and CO_2, determined by an internal standard method using N_2, was 98.5–99.5% in the POM by Rh–Co/MOR under our reaction conditions. No other carbon-containing products were observed except for a trace amount of coke, quantified with a total organic carbon analyser (TOC-V_{CSN}, Shimadzu). Therefore, selectivity for CO was defined as the ratio of $CO/(CO + CO_2)$ to obtain better accuracy even at low conversions of methane. Details of the calculations are available in Supplementary Note 1.

Data availability. Data that support the findings of this study are available from the corresponding author upon reasonable request.

Received: 13 April 2018 Accepted: 13 July 2018
Published online: 01 August 2018

References

1. Wang, Q., Chen, X., Jha, A. N. & Rogers, H. Natural gas from shale formation—the evolution, evidences and challenges of shale gas revolution in United States. *Renew. Sustain. Energy Rev.* **30**, 1–28 (2014).
2. Karakaya, C. & Kee, R. J. Progress in the direct catalytic conversion of methane to fuels and chemicals. *Prog. Energy Combust. Sci.* **55**, 60–97 (2016).
3. Tomkins, P., Ranocchiari, M. & van Bokhoven, J. A. Direct conversion of methane to methanol under mild conditions over Cu-zeolites and beyond. *Acc. Chem. Res.* **50**, 418–425 (2017).
4. Ogo, S. & Sekine, Y. Catalytic reaction assisted by plasma or electric field. *Chem. Rec.* **17**, 726–738 (2017).
5. Luk, H. T., Mondelli, C., Ferré, D. C., Stewart, J. A. & Pérez-Ramírez, J. Status and prospects in higher alcohols synthesis from syngas. *Chem. Soc. Rev.* **46**, 1358–1426 (2017).
6. Tang, M., Xu, L. & Fan, M. Progress in oxygen carrier development of methane-based chemical-looping reforming: A review. *Appl. Energy* **151**, 143–156 (2015).
7. Aasberg-Petersen, K. et al. Technologies for large-scale gas conversion. *Appl. Catal. A Gen.* **221**, 379–387 (2001).
8. Horn, R. & Schlögl, R. Methane activation by heterogeneous catalysis. *Catal. Lett.* **145**, 23–39 (2015).
9. Kraus, P. & Lindstedt, R. P. Microkinetic mechanisms for partial oxidation of methane over platinum and rhodium. *J. Phys. Chem. C* **121**, 9442–9453 (2017).
10. Urasaki, K. et al. Synthesis gas production by catalytic partial oxidation of natural gas using ceramic foam catalyst. *Catal. Today* **299**, 219–228 (2018).
11. Eriksson, S., Rojas, S., Boutonnet, M. & Fierro, J. L. G. Effect of Ce-doping on Rh/ZrO_2 catalysts for partial oxidation of methane. *Appl. Catal. A Gen.* **326**, 8–16 (2007).
12. Hou, Y., Ogasawara, S., Fukuoka, A. & Kobayashi, H. Zeolite-supported rhodium sub-nano cluster catalyst for low-temperature selective oxidation of methane to syngas. *Catal. Sci. Technol.* **7**, 6132–6139 (2017).
13. Choudhary, V. R., Rajput, A. M., Prabhakar, B. & Mamman, A. S. Partial oxidation of methane to CO and H_2 over nickel and/or cobalt containing ZrO_2, ThO_2, UO_2, TiO_2 and SiO_2 catalysts. *Fuel* **77**, 1803–1807 (1998).
14. Xia, W. et al. Partial oxidation of methane into syngas (H_2+CO) over effective high-dispersed Ni/SiO_2 catalysts synthesized by a sol–gel method. *Int. J. Hydrogen Energy* **37**, 8343–8353 (2012).
15. Dedov, A. G. et al. Partial oxidation of methane to produce syngas over a neodymium–calcium cobaltate-based catalyst. *Appl. Catal. A Gen.* **489**, 140–146 (2015).
16. Basile, F., Fornasari, G., Trifirò, F. & Vaccari, A. Rh–Ni synergy in the catalytic partial oxidation of methane: surface phenomena and catalyst stability. *Catal. Today* **77**, 215–223 (2002).
17. Naito, S. et al. Promoting effect of Co addition on the catalytic partial oxidation of methane at short contact time over a Rh/MgO catalyst. *J. Catal.* **259**, 138–146 (2008).
18. Cesar, D. V. et al. Stability of Ni and Rh–Ni catalysts derived from hydrotalcite-like precursors for the partial oxidation of methane. *Int. J. Hydrogen Energy* **38**, 5616–5626 (2013).
19. Berger-Karin, C., Radnik, J. & Kondratenko, E. V. Mechanistic origins of the promoting effect of tiny amounts of Rh on the performance of NiO_x/Al_2O_3 in partial oxidation of methane. *J. Catal.* **280**, 116–124 (2011).
20. Roh, H.-S., Jun, K.-W., Baek, S.-C. & Park, S.-E. A highly active and stable catalyst for carbon dioxide reforming of methane: $Ni/Ce–ZrO_2/q\text{-}Al_2O_3$. *Catal. Lett.* **81**, 147–151 (2002).
21. Chai, J. W. et al. Thermal behaviour of ultra-thin Co overlayers on rutile TiO_2(100) surface. *Surf. Sci.* **589**, 32–41 (2005).
22. Dominguez, M., Taboada, E., Idriss, H., Molins, E. & Llorca, J. Fast and efficient hydrogen generation catalyzed by cobalt talc nanolayers dispersed in silica aerogel. *J. Mater. Chem.* **20**, 4875–4883 (2010).
23. Tan, B. J., Klabunde, K. J. & Sherwood, P. M. A. XPS studies of solvated metal atom dispersed (SMAD) catalysts. Evidence for layered cobalt-manganese particles on alumina and silica. *J. Am. Chem. Soc.* **113**, 855–861 (1991).
24. Lónyi, F., Solt, H. E., Pászti, Z. & Valyon, J. Mechanism of NO-SCR by methane over Co,H-ZSM-5 and Co,H-mordenite catalysts. *Appl. Catal. B* **150**, **151**, 218–229 (2014).
25. Kim, D. J. et al. Enhancement in the reducibility of cobalt oxides on a mesoporous silica supported cobalt catalyst. *Chem. Commun.* 1462–1464 (2005).
26. Takenaka, S., Ishida, M., Serizawa, M., Tanabe, E. & Otsuka, K. Formation of carbon nanofibers and carbon nanotubes through methane decomposition over supported cobalt catalysts. *J. Phys. Chem. B* **108**, 11464–11472 (2004).
27. Lapidus, A. et al. Hydrocarbon synthesis from carbon monoxide and hydrogen on impregnated cobalt catalysts. Part I. Physico-chemical properties of 10% cobalt/alumina and 10% cobalt/silica. *Appl. Catal.* **73**, 65–81 (1991).
28. Mimeault, V. J. & Hansen, R. S. Flash desorption and isotopic mixing of hydrogen and deuterium adsorbed on tungsten, iridium, and rhodium. *J. Phys. Chem.* **45**, 2240–2250 (1966).
29. Im, J., Shin, H., Jang, H., Kim, H. & Choi, M. Maximizing the catalytic function of hydrogen spillover in platinum-encapsulated aluminosilicates with controlled nanostructures. *Nat. Commun.* **5**, 3370 (2014).
30. Lee, S., Lee, K., Im, J., Kim, H. & Choi, M. Revisiting hydrogen spillover in Pt/LTA: effects of physical diluents having different acid site distributions. *J. Catal.* **325**, 26–34 (2015).
31. Tanaka, H., Kaino, R., Okumura, K., Kizuka, T. & Tomishige, K. Catalytic performance and characterization of $Rh–CeO_2/MgO$ catalysts for the catalytic partial oxidation of methane at short contact time. *J. Catal.* **268**, 1–8 (2009).

Acknowledgements

We thank Ms. N. Hirai (technical division) for taking the STEM images. This work was supported by Japan Science and Technology Agency (JST) CREST Grant Number JPMJCR15P4. The Open Facility of Institute for Catalysis was utilised for the XPS and TEM measurements.

Author contributions

Y.H. performed POM and characterisations. S.N. and K.A. measured XAFS spectra and assisted in their analysis. Y.H., H.K., and A.F. wrote the manuscript. H.K. conducted the project with the advice of A.F.

Additional information

Supplementary information accompanies this paper at https://doi.org/10.1038/s42004-018-0044-9.

Competing interests: The authors declare no competing interests.

Reprints and permission information is available online at http://npg.nature.com/reprintsandpermissions/

Publisher's note: Springer Nature remains neutral with regard to jurisdictional claims in published maps and institutional affiliations.